Supplementary Materials

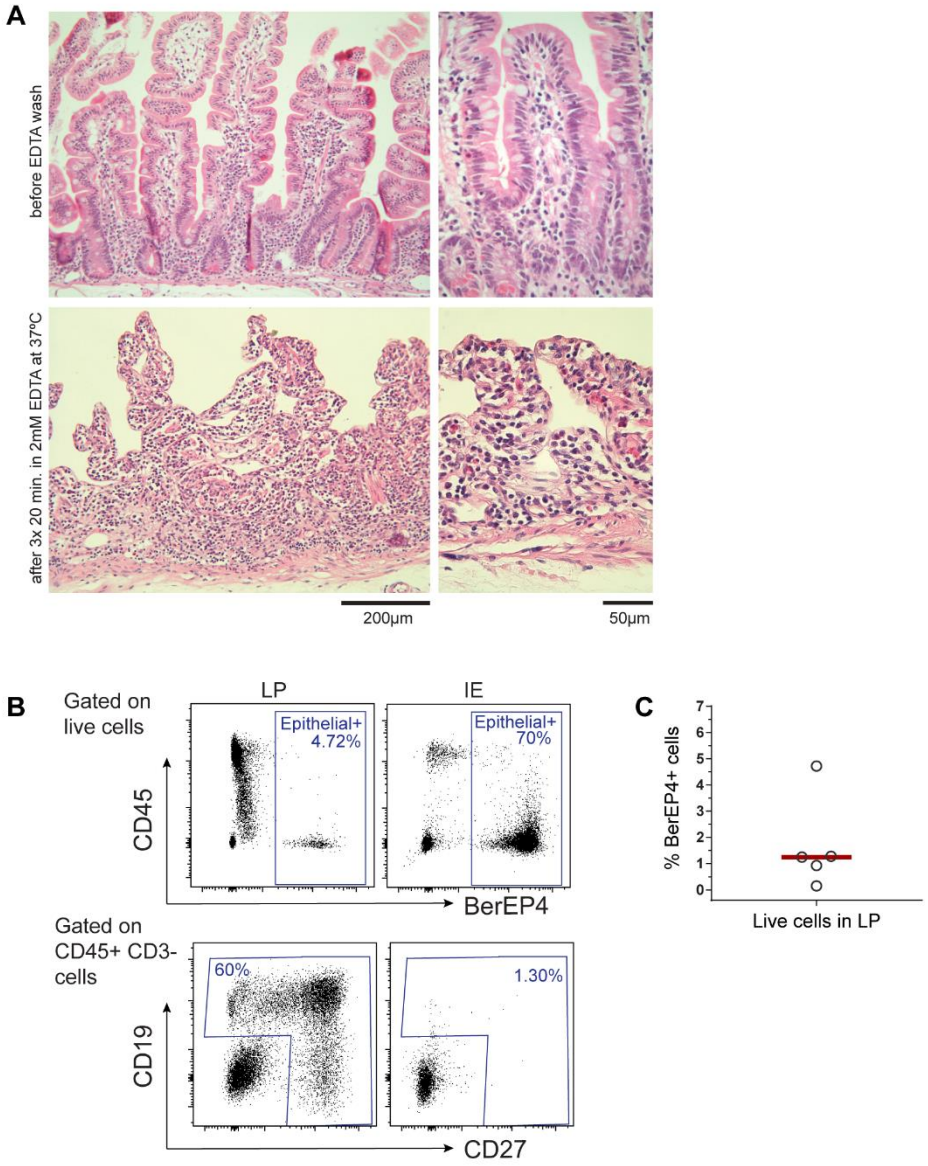

Figure S1. Confirmation of the absence of cross-contamination between LP and IE tissue fractions. (**A**) Representative hematoxylin-eosin (H/E) staining of tissue sections obtained before and after three sequential washing steps with EDTA buffer (PBS containing 2mM EDTA and 1%FCS) at 37°C with vigorous shaking. (**B**) Representative flow cytometric plot showing the percentage of epithelial cells (BerEP4+ cells) and B cells within each fraction. (**C**) Compile data for the percentage of epithelial cells (BerEP4+ cells) remaining in the LP after three sequential washing steps with EDTA buffer.

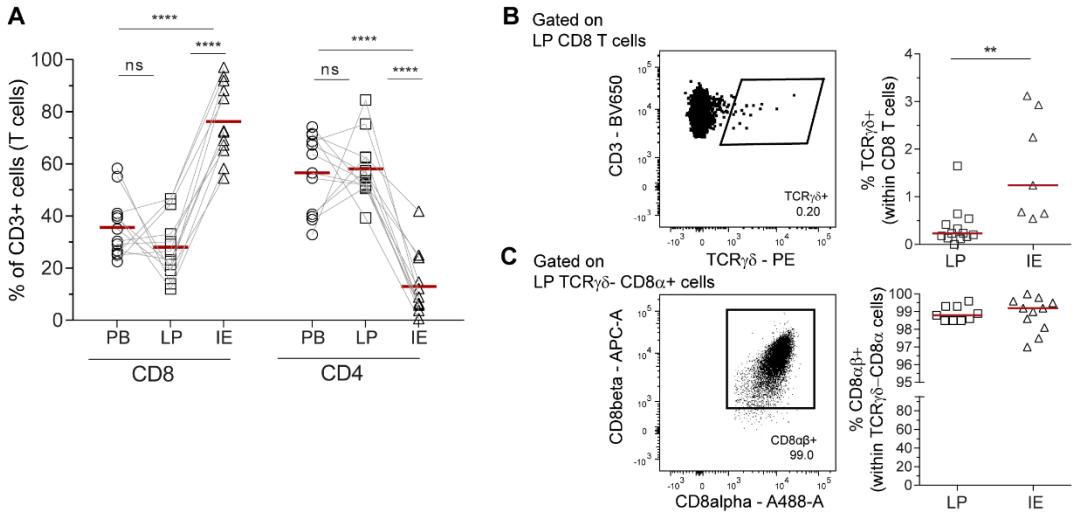

Figure S2. (**A**). Percentage of T cell subsets (CD4 and CD8) in peripheral blood (PB), lamina propria (LP) and epithelium(IE) measured by flow cytometry. Red line indicates mean value. Statistics performed using two-ways ANOVA, repeated measures (RM) matching both factors, and Turkey's multiple comparison test. (**B**) TCRγδ and (**C**) CD8β expression on LP and IE CD8 T cells analyzed by flow cytometry. Red line indicates median value. Unpaired T-test. **P≤0.01.

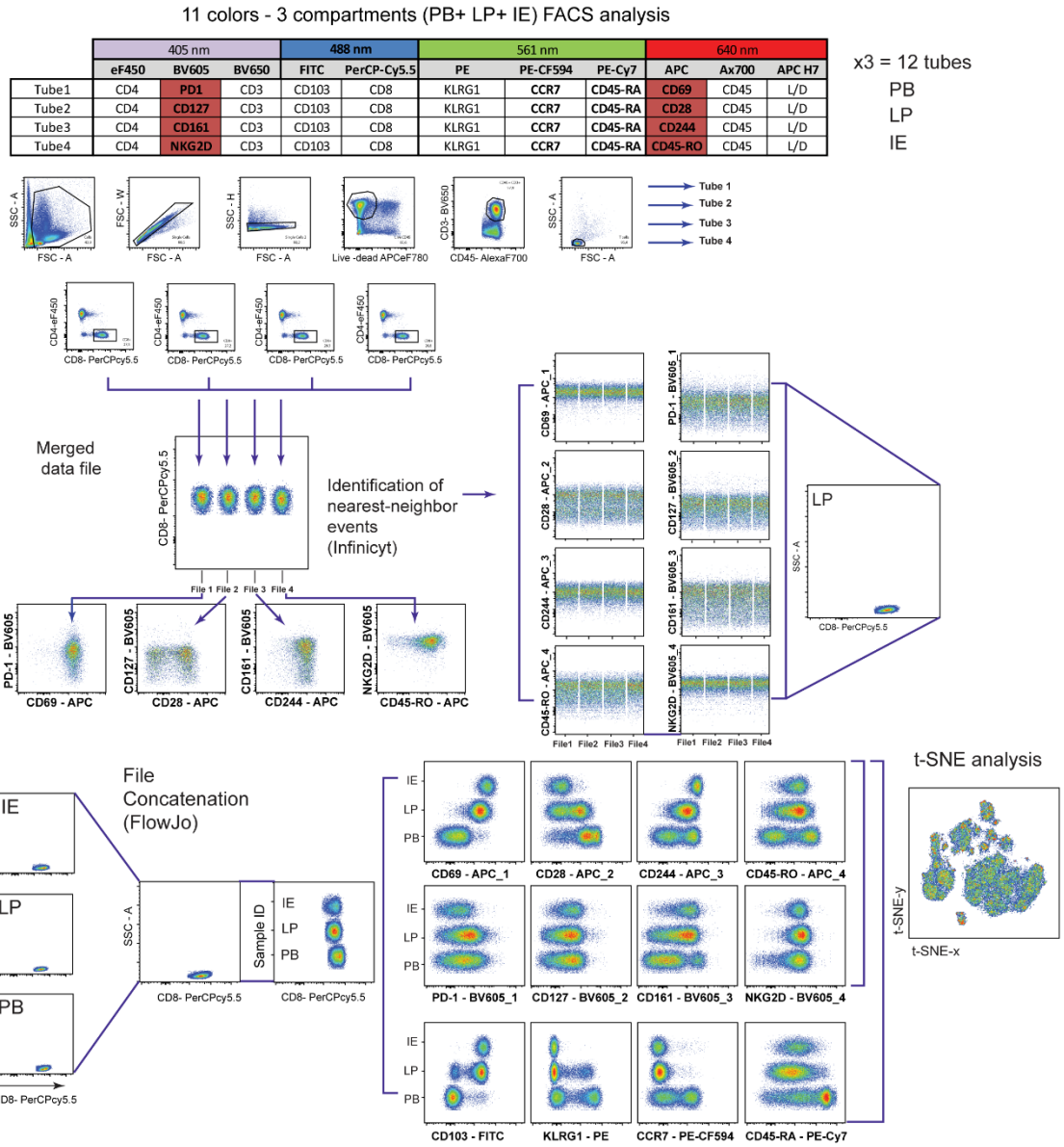

Figure S3. Related to Figure 1C. Panel design, merge (as described in (Pedreira et al., 2008a; Pedreira et al., 2008b)) and concatenation of flow cytometric files before applying t-SNE analysis (FlowJo plugin).

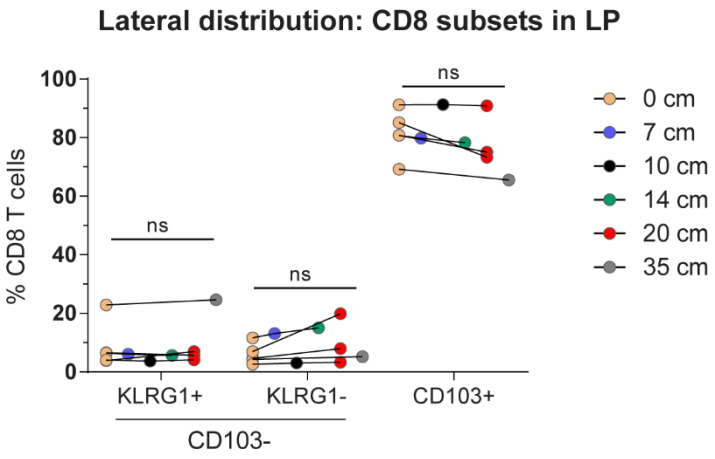

Figure S4. Lateral distribution of LP CD8 T cell subsets. The lengthwise representation of the CD8 subsets in LP was determined by flow cytometric analysis of biopsies taken at intervals along resected duodenum-proximal jejunum from individual subjects after Whipple procedure. n = 5; paired Student's t test comparing 0 cm –furthest distance. ns, not significant.

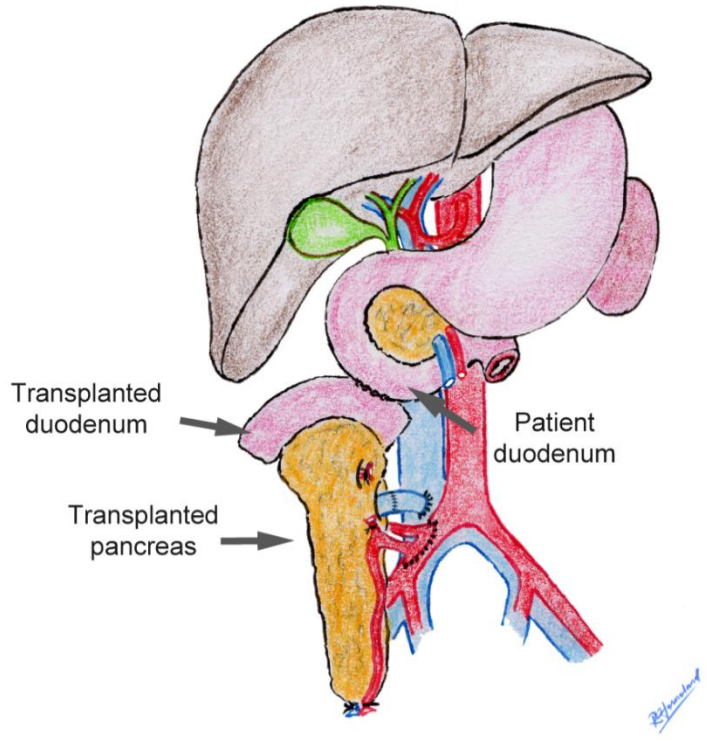

Figure S5. Representation of the pancreas transplantation showing the duodeno-duodenostomy anastomosis, as described in (Horneland et al., 2015).

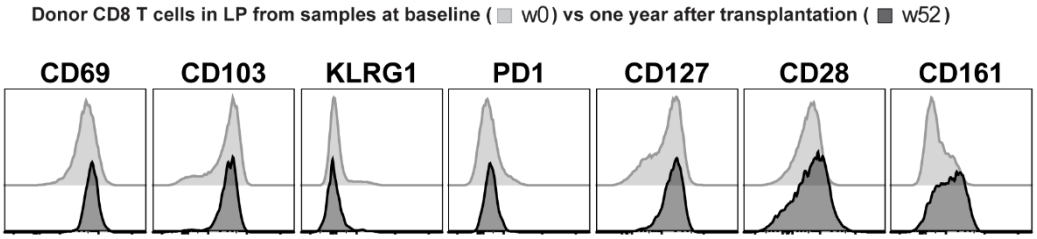

Figure S6. The expression profile of donor LP CD8 T cells derived from duodenal transplant at baseline (w0) vs one-year after transplantation (w52).

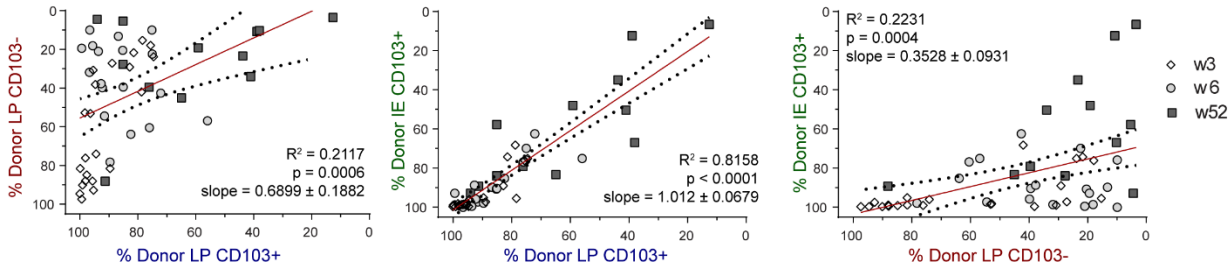

Figure S7. Correlation of replacement kinetics for donor CD103-, LP and IE CD103+ CD8 T cell subsets. Statistics performed using Pearson correlation with two-tailed p-value (95% confidence interval).

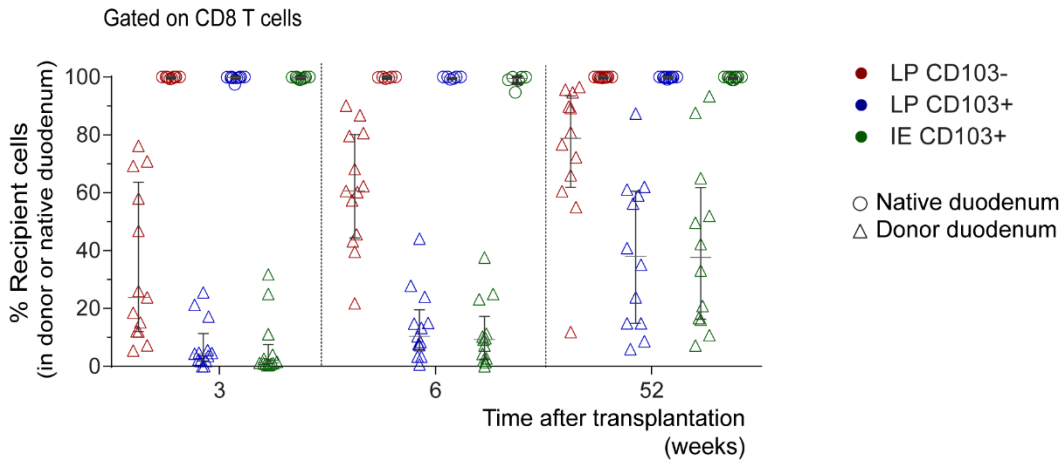

Figure S8. Percentage of recipient CD8 T cells for each subset isolated from donor and recipient (native) duodenum of the same patients at different time points post-transplantation.

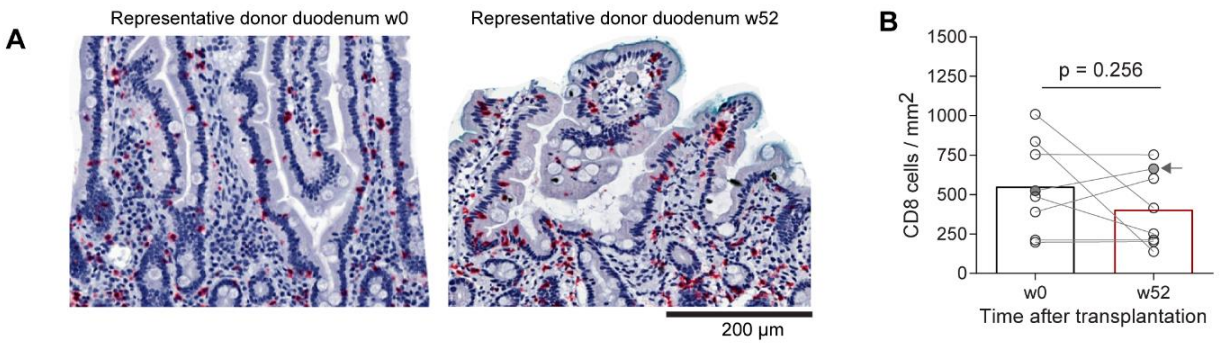

Figure S9. (A) Representative immunohistochemistry staining of CD8 T cells (Fast-Red) on tissue sections from donor duodenum of a representative patient before (w0) and 1-year post-Tx (w52). **(B)** Total CD8 T cell counts on tissue sections from donor duodenum of representative patients (n=8) before (w0) and 1-year post-Tx (w52). The patient shown in (A) is filled in gray and pointed with an arrow. Paired T-test.

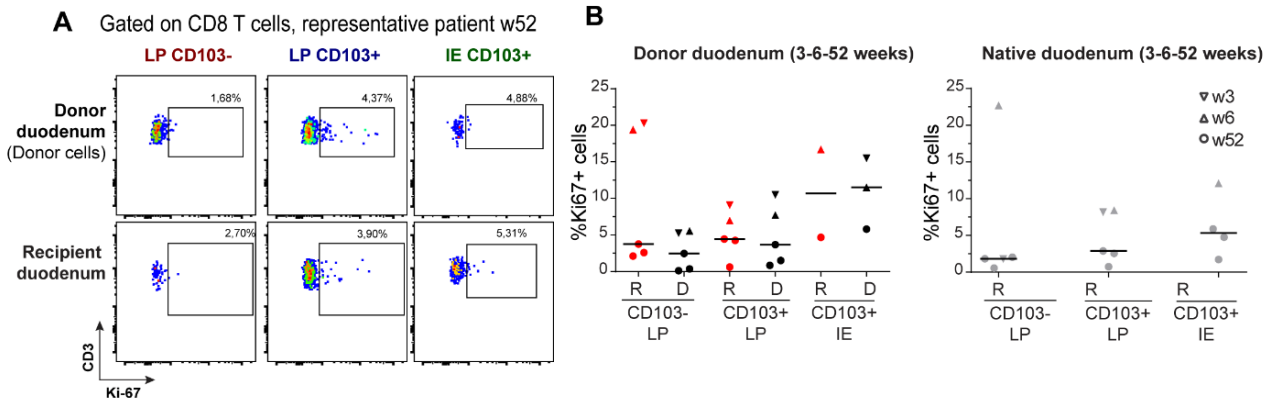

Figure S10. (A) Representative dot plot of Ki67 expression in CD8 T cell subsets derived from a donor and native duodenum one-year post-transplantation. **(B)** Compiled data for the percentage of CD8 T cell subsets expressing Ki67 at different time points after transplantation in donor and native duodenum.

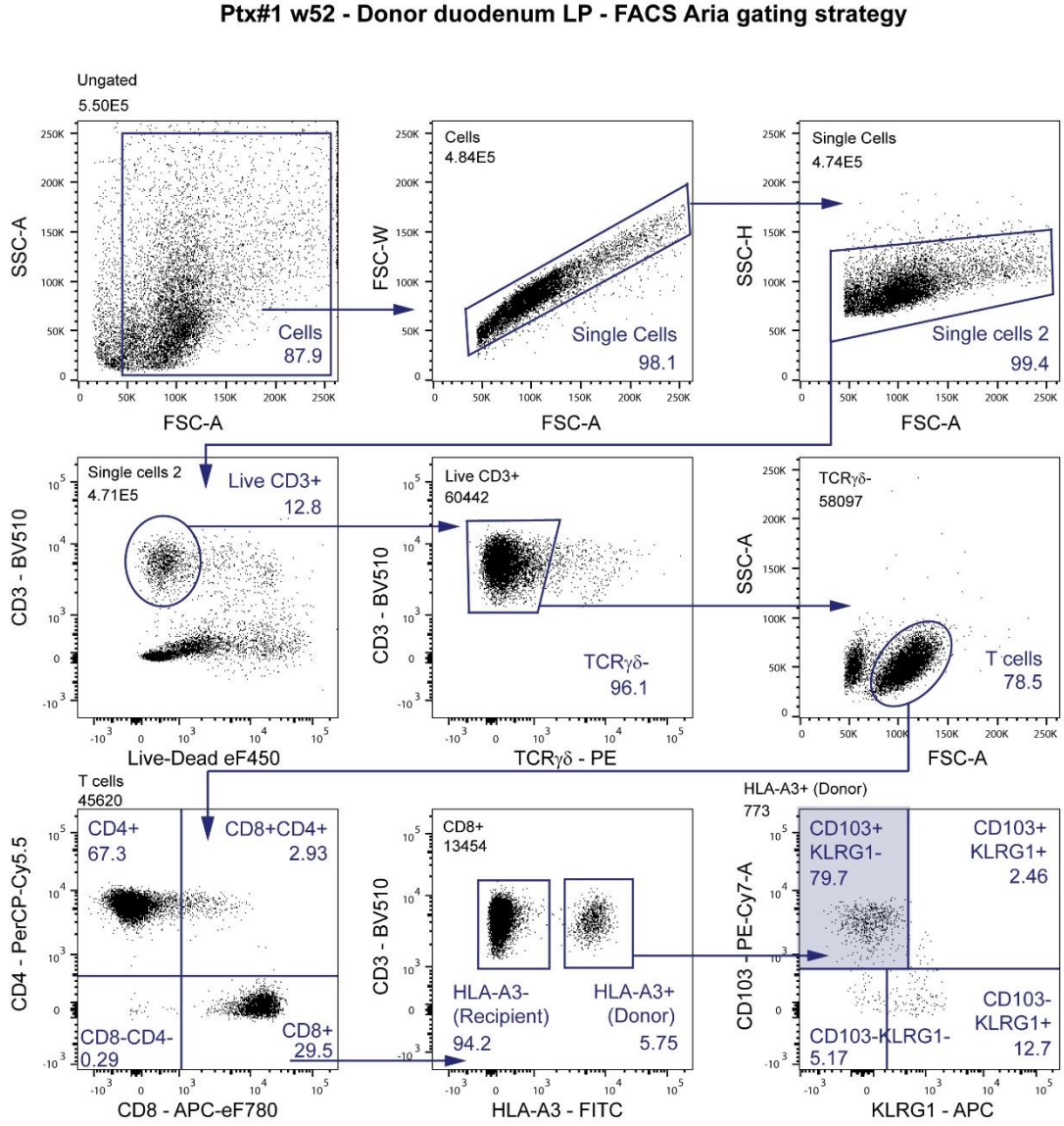

Figure S11. Gating strategy for single cell sorting of CD8 T cells from duodenal biopsies. Representative sample of grafted duodenum from a transplanted patient one-year after transplantation is shown.

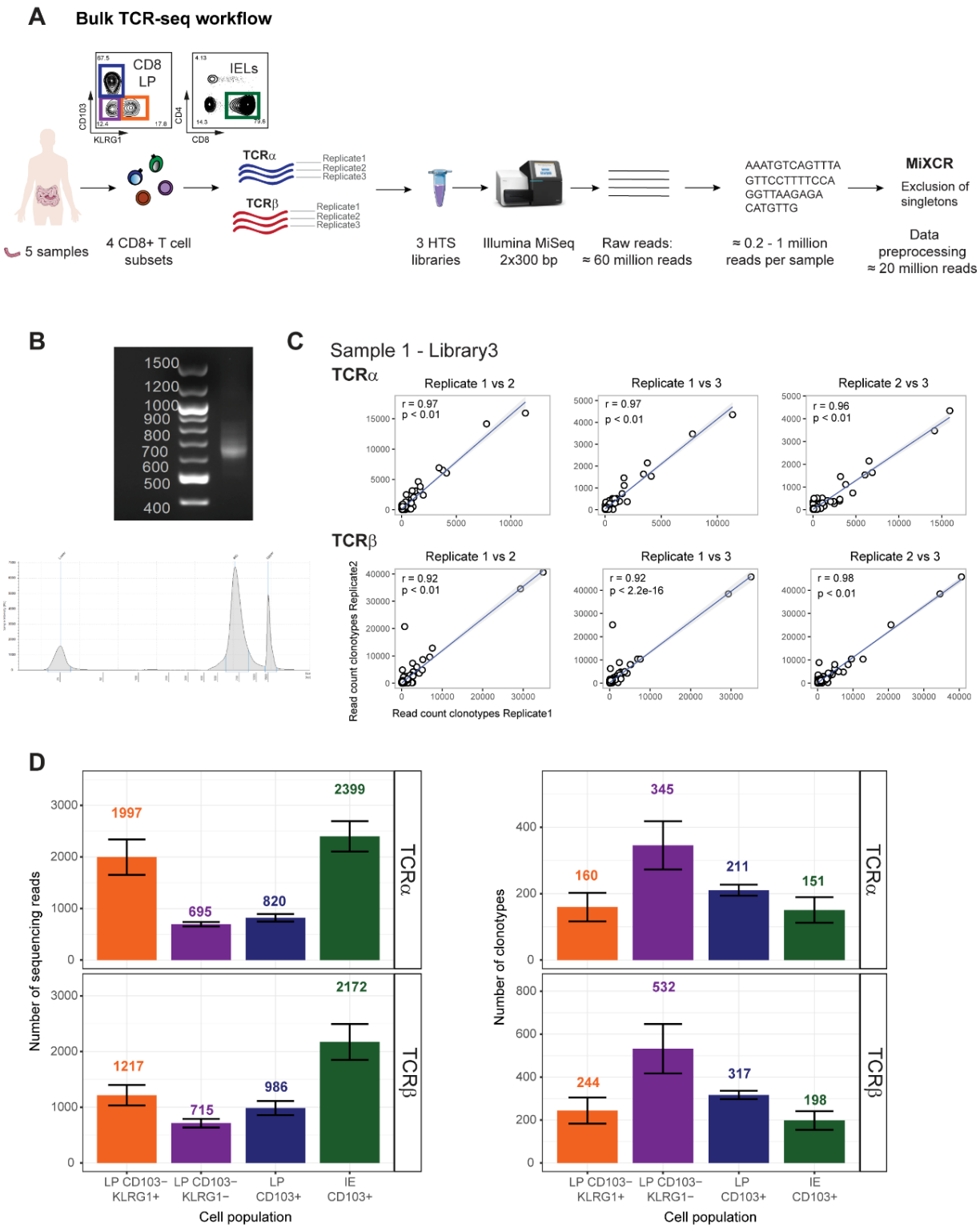

Figure S12. Bulk TCR-seq workflow and read statistics. (**A**) Overview of sample processing, data acquisition and data processing. (**B**) Agarose gel shows representative library following the protocol explained in (A). Expected band size ≈700 bp. (**C**) Correlation plots showing the correlation of the common clonotypes between the three replicates representative sample. (**D**) Clone and sequence counts after MiXCR preprocessing are shown by CD8 T cell subset (mean ± s.e.m). The total number of sequencing reads used for the analysis was 20,692,061 (total number of raw reads: ≈ 62,317,193). Mean Phred scores of raw data were ≥30.

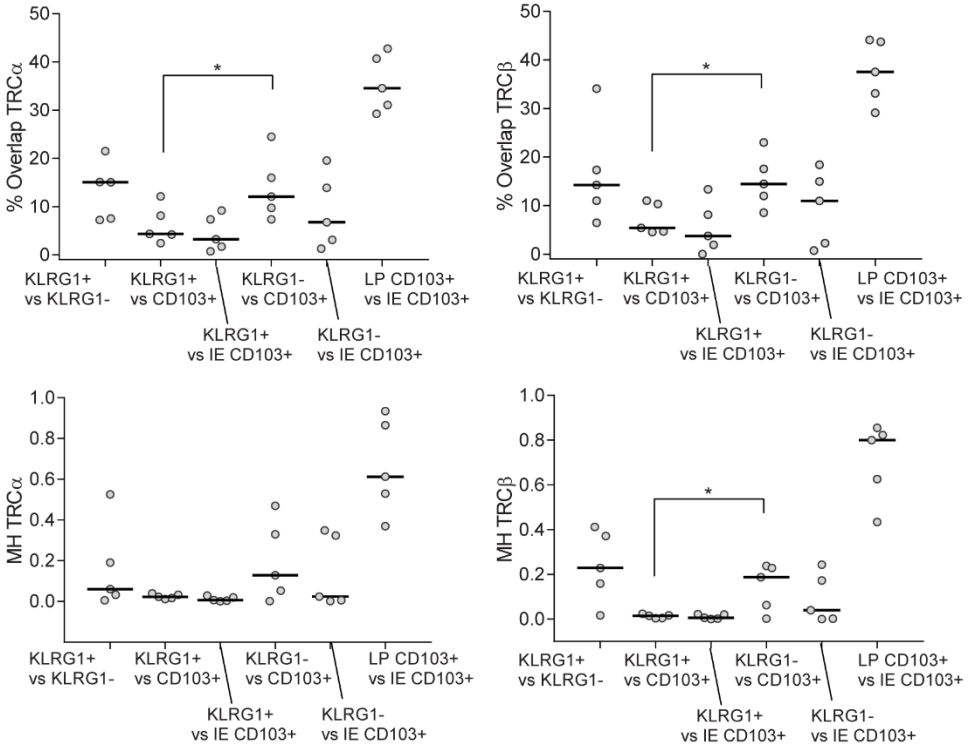

Figure S13. Compiled data of pairwise clonal overlap and Morisita-Horn calculation for the TCRα and TCRβ clonotypes in all the samples. Paired t-test, two-tailed; *P≤0.05, n.s., not significant.

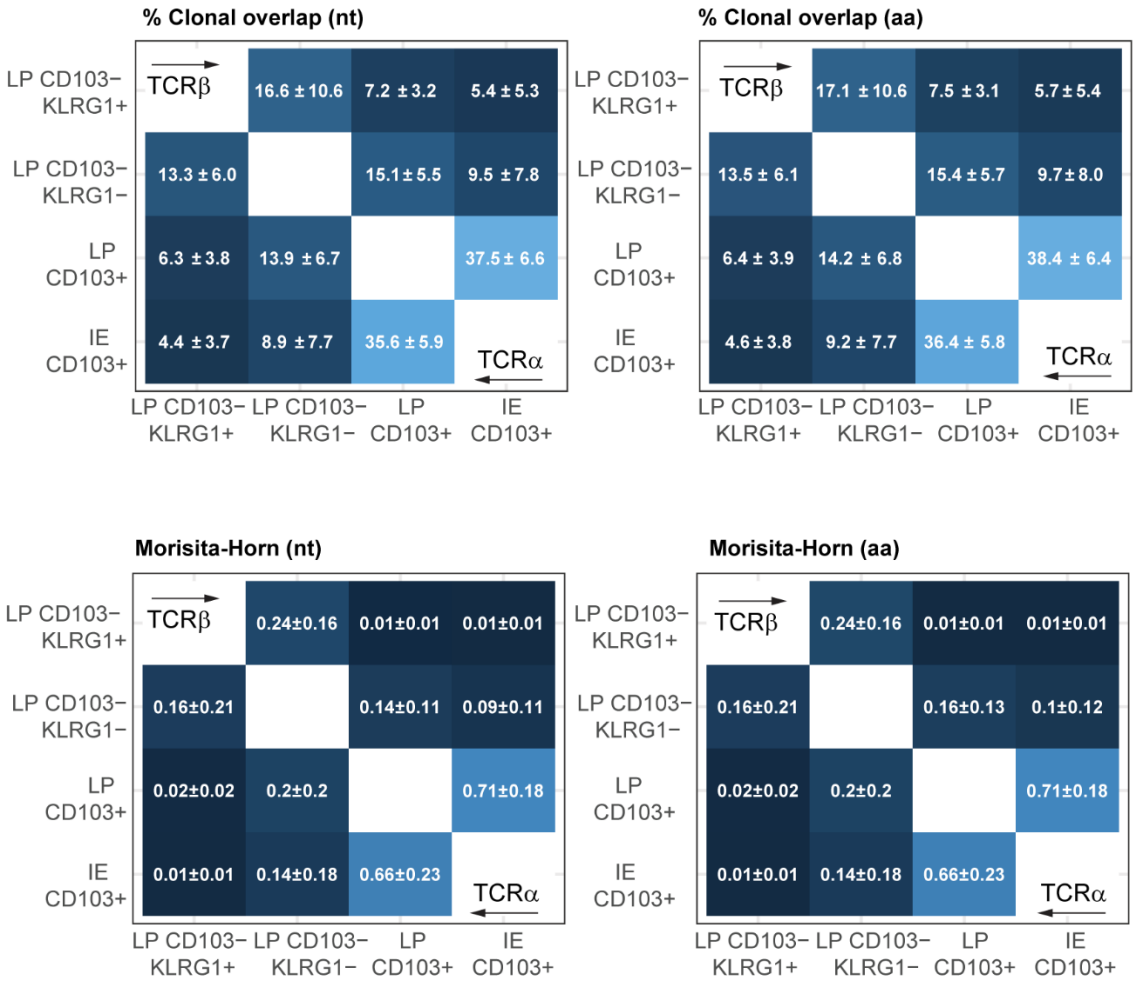

Figure S14. Pairwise clonal overlap and Morisita-Horn calculation for the TCRα and TCRβ clonotypes in all the samples. Similar values were found when the amino acid sequence (aa) of the CDR3 was used as the clonotype definition instead of the nucleotide sequence (nt).

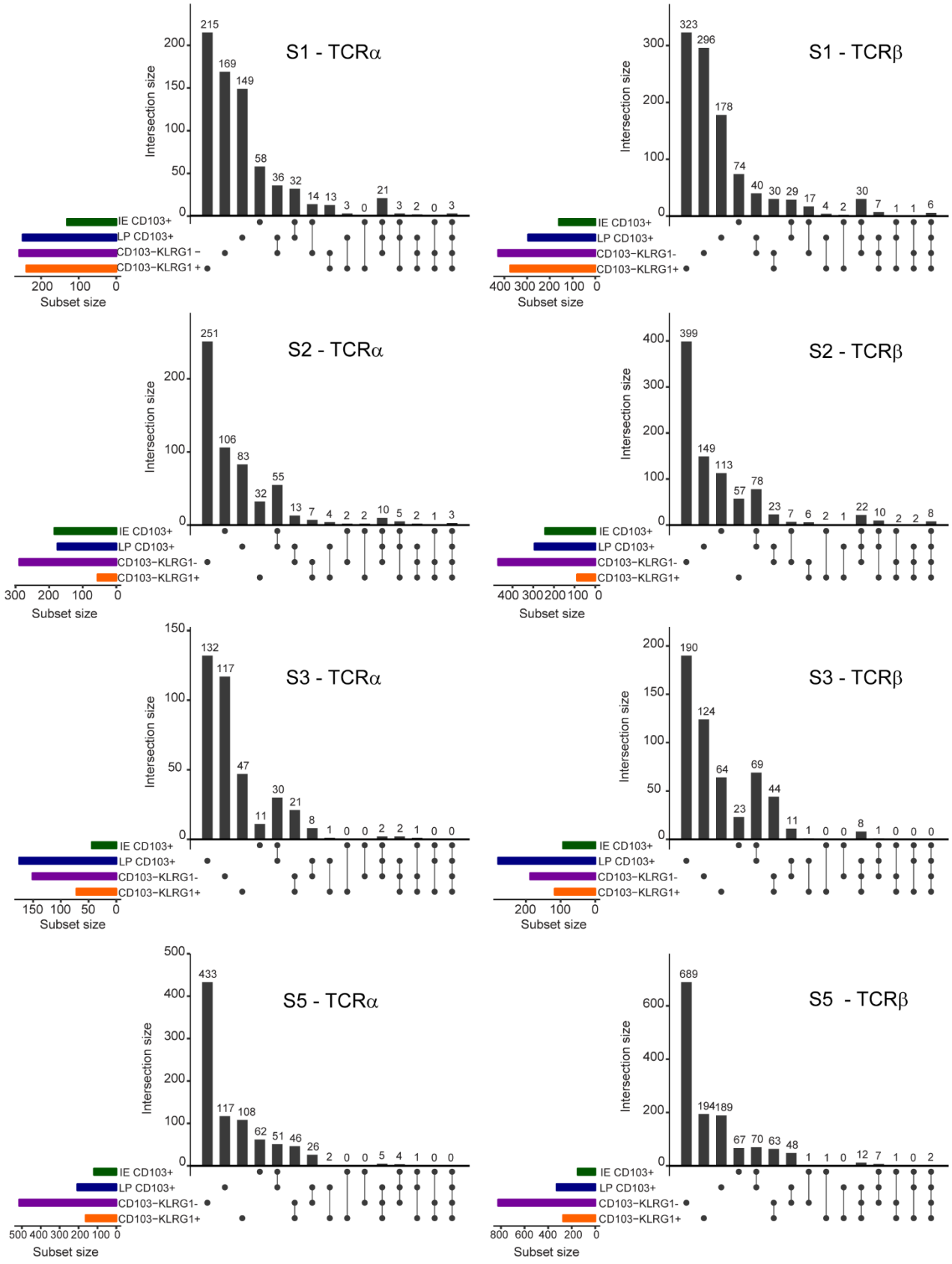

Figure S15. Upset plots with the overlapping clones for TCRα and TCRβ in all the samples analyzed.

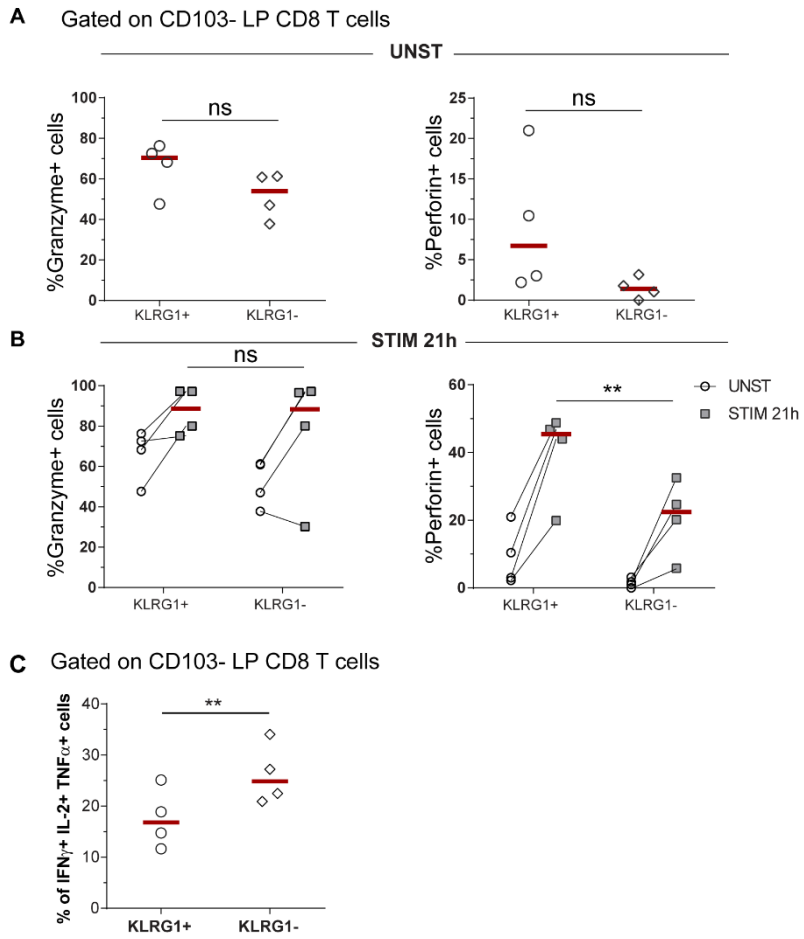

Figure S16. Percentage of Granzyme and perforin positive cells in unstimulated samples (**A)** and after 21h of activation with anti-CD3 beads (**B)** for the different CD103- CD8 T cell subsets (KLRG1+, KLRG1-) in LP. (**C)** Percentage of polyfunctional (IL-2+, IFN-γ+ and TNF-α+) cells for the different CD103- CD8 T cell subsets (KLRG1+, KLRG1-) in LP.

Table S1. List of antibodies used in the study

Target	Clone	Fluorophore	Company	Cat. num	Phenotype Trm	PTx panel	Aria Sorting	Ki67 nuclear	Cytotoxicity	Cytokines	X/Y - FISH
CD3	OKT_3	BV650	Biolegend	317324	x	x		x			
CD3	OKT_3	APC-eF780	eBioscience	47-0037-42			x			x	
CD3	OKT_3	BV510	Biolegend	317332						x	
CD3	OKT_3	APC	Biolegend	317318			x				
CD3	OKT_3	PerCP-Cy5.5	Biolegend	317336				x			
CD3	Poly	unconjugated	Dako	A0452							x
CD4	OKT_4	eF450	eBioscience	48-0048-42	x	x		x		x	
CD4	OKT_4	PerCP-Cy5.5	Biolegend	317428			x				
CD8	SK1	Alexa-Fluor488	Biolegend	344716	x	x					
CD8	SK1	APC-eF780	eBioscience	47-0087-42			x		x	x	
CD8	SK1	PerCP Cy5.5	Biolegend	344710	x					x	
CD8	SK1	PE	BD Biosciences	340046				x			
CD8	4B11	unconjugated	Novocastra	NCL-L-CD8-4B11							x
CD8b /NHP	SIDI8BEE	eF660	eBioscience	50-5273-41	x	x					
CD28	CD28.2	BV605	BD Horizon	562976	x	x					
CD28	CD28.2	APC	Biolegend	302912	x	x					
CD28	CD28.2	PE	Biolegend	302908	x	x					
CD45	HI30	BV510	Biolegend	304036			x	x	x		
CD45	HI30	Ax700	Biolegend	304024	x						
CD45	2D1	APC-H7	BD-Biosciences	560178	x	x				x	
CD45-RA	HI100	APC-eF780	eBioscience	47-0458-42	x					x	
CD45-RA	HI100	PE-Cy7	eBioscience	25-0458-42			x			x	
CD45-RO	UCHL1	APC	eBioscience	17-0457-42							
CD103	B-Ly7	PE-Cy7	Biolegend	350212	x	x	x	x	x		
CD103	Ber-ACT8	BV605	Biolegend	350218						x	
CD103	Ber-ACT8	PE-Cy7	Biolegend	350212						x	
CD103	B-Ly7	FITC	eBioscience	11-1038-42	x						
CD62-L (L-Sel)	SK11	FITC	BD Pharmingen	347443	x						
CD127 (IL7-R)	Hil7r-m21	PE	BD Pharmingen	561028	x	x				x	
CD127 (IL7-R)	Hil7r-m21	BV605	BD Horizon	562662	x	x					
CD161 (KLRB1)	HP-3G10	BV605	Biolegend	339915	x	x					
CD244 (SLAMF4)	2B4	APC	Biolegend	329511	x	x					
CCR7 (CD197)	G043H7	PE	Biolegend	353203	x						
CCR7 (CD197)	G043H7	PE-dazzle594	Biolegend	353235	x						
PD-1 (CD279)	EH12.1	BV605	BD Horizon	563245	x	x					
KLRG1	13F12F2	APC	eBioscience	17-9488-42	x	x	x	x	x	x	
KLRG1	13F12F2	PE	eBioscience	12-9488-42	x	x	x		x		
NKG2D	1D11	PE	Biolegend	320805	x	x					
NKG2D	1D11	BV605	BD Biosciences	743559	x	x					
TCR-gd	5A6.E9	PE	Molecular Probes™, Invitrogen	MHGD04	x	x	x				
TCR-gd	5A6.E9	FITC	Molecular Probes™, Invitrogen	MHGD01		x	x				
Anti-Human Epithelial Antigen	Ber-EP4	FITC	Dako	F0860			x				
HLA-A2	BB 7.2	PE	Abcam	ab79523		x					
HLA-A3	GAP.A3	FITC	eBioscience	11-5754-42		x					
HLA-A3	GAP.A3	APC	eBioscience	17-5754-42		x	x				
HLA-B7	BB7.1	PE	Millipore	MAB1288		x					
HLA-B8	REA145	PE	Miltenyi Biotech	130-118-960		x	x				
Granzyme-B	CLB-GB11	PE	SANQUIN (Dianova AS)	M2289					x		
Perforin	gG9	FITC	BD Pharmingen	556577					x		
TNF-alpha	MAb11	APC	Biolegend	502912						x	
IFNg	4S.B3	Ax488	Biolegend	502515						x	
IL2	MQ1-17H12	PE	Biolegend	500307						x	
IL2	MQ1-17H12	BV421	Biolegend	500327						x	
MIP1beta (CCL4)	FL3423L	APC	eBioscience	17-7540-41						x	
Ki67	B56	Ax488	BD Pharmingen	558616				x			
Isotype mouse IgG1	MOPC-21	Ax488	BD Pharmingen	555909				x	x		
Isotype mouse IgG2b	27-35	FITC	BD Pharmingen	556577					x		
Isotype mouse IgG1	MOPC-31C	PE	BD Pharmingen	550617					x		
Mouse IgG2b	Poly	Alexa 555	Molecular Probes™, Invitrogen	A-21147							x
Rabbit IgG (H+L)	Poly	Alexa 647	Molecular Probes™, Invitrogen	A-31573							x

References and Notes:

Horneland, R., Paulsen, V., Lindahl, J.P., Grzyb, K., Eide, T.J., Lundin, K., Aabakken, L., Jenssen, T., Aandahl, E.M., Foss, A., and Oyen, O. (2015). Pancreas transplantation with enteroanastomosis to native duodenum poses technical challenges--but offers improved endoscopic access for scheduled biopsies and therapeutic interventions. Am J Transplant *15*, 242-250.

Pedreira, C.E., Costa, E.S., Arroyo, M.E., Almeida, J., and Orfao, A. (2008a). A multidimensional classification approach for the automated analysis of flow cytometry data. IEEE Trans Biomed Eng *55*, 1155-1162.

Pedreira, C.E., Costa, E.S., Barrena, S., Lecrevisse, Q., Almeida, J., van Dongen, J.J., Orfao, A., and EuroFlow, C. (2008b). Generation of flow cytometry data files with a potentially infinite number of dimensions. Cytometry A *73*, 834-846.